REPORT DOCUMENTATION PAGE

Form Approved
OMB No. 0704-0188

PLEASE DO NOT RETURN YOUR FORM TO THE ABOVE ORGANIZATION.

1. REPORT DATE *(DD-MM-YYYY)*	2. REPORT TYPE	3. DATES COVERED *(From - To)*
03-07-2013	Journal Article	

4. TITLE AND SUBTITLE
Configuring High Frequency Radar Observations in the Southern Chukchi Sea

5a. CONTRACT NUMBER

5b. GRANT NUMBER

5c. PROGRAM ELEMENT NUMBER
0602435N

6. AUTHOR(S)
Gleb Panteleev, Max Yaremchuk, Oceana Francis and Takashi Kikuchi

5d. PROJECT NUMBER

5e. TASK NUMBER

5f. WORK UNIT NUMBER
73-6414-02-5

7. PERFORMING ORGANIZATION NAME(S) AND ADDRESS(ES)
Naval Research Laboratory
Oceanography Division
Stennis Space Center, MS 39529-5004

8. PERFORMING ORGANIZATION REPORT NUMBER
NRL/JA/7320--12-1340

9. SPONSORING/MONITORING AGENCY NAME(S) AND ADDRESS(ES)
Office of Naval Research
One Liberty Center
875 North Randolph Street, Suite 1425
Arlington, VA 22203-1995

10. SPONSOR/MONITOR'S ACRONYM(S)
ONR

11. SPONSOR/MONITOR'S REPORT NUMBER(S)

12. DISTRIBUTION/AVAILABILITY STATEMENT
Approved for public release, distribution is unlimited.

13. SUPPLEMENTARY NOTES

14. ABSTRACT

In recent years, monitoring offshore surface circulation in the Arctic Ocean with high frequency radars has become an issue of increasing practical importance. In this study, radar positions are optimized by minimizing the reconstruction errors of the surface currents in the Southeastern Chukchi Sea. By means of an adjoint sensitivity technique it is shown that in the case of a pair of radars, their optimal (i.e. most favorable) location is at Kivalina, a settlement near the strongest outflow of the Alaskan Coastal Current from the monitored domain. The least favorable location is at Shishmaref, a settlement near relatively weak inflow into the region as observed from the coast. However, if two pairs of radars are available, the best locations are Kivalina and Shishmaref. The results are verified using observational system simulation experiments (OSSEs) performed in the framework of a 4-dimensional variational assimilation of simulated radar observations into a numerical model. It is shown that correct specification of the first guess solution is of primary importance for obtaining realistic results from both adjoint sensitivity analysis and OSSEs. This emphasizes the necessity of obtaining accurate high resolution climatologies for future ice-free offshore regions in the Arctic.

15. SUBJECT TERMS
data assimilation, optimization, Chukchi Sea, high frequency radar

16. SECURITY CLASSIFICATION OF:			17. LIMITATION OF ABSTRACT	18. NUMBER OF PAGES	19a. NAME OF RESPONSIBLE PERSON
a. REPORT	b. ABSTRACT	c. THIS PAGE			Max Yaremchuk
Unclassified	Unclassified	Unclassified	UU	10	19b. TELEPHONE NUMBER *(Include area code)* (228) 688-5259

Reset

Standard Form 298 (Rev. 8/98)
Prescribed by ANSI Std. Z39.18

Available online at www.sciencedirect.com

SciVerse ScienceDirect

Polar Science 7 (2013) 72–81

http://ees.elsevier.com/polar/

Configuring high frequency radar observations in the Southern Chukchi Sea

Gleb Panteleev [a,*], Max Yaremchuk [b], Oceana Francis [c], Takashi Kikuchi [d]

[a] International Arctic Research Center, PO Box 757340, University of Alaska Fairbanks, Fairbanks, AK 99775, USA
[b] Naval Research Laboratory, NRL Code 7320, Building 1009, Stennis Space Center, MS 39529, USA
[c] Department of Civil and Environmental Engineering, University of Hawaii at Manoa, 2540 Dole Street, Holmes Hall 383, Honolulu, HI 96822, USA
[d] Japan Agency for Marine-Earth Science and Technology, 3173-25, Showa-machi, Kanazawa-ku, Yokohama-city, Kanagawa 236-0001, Japan

Received 8 August 2012; revised 4 December 2012; accepted 29 January 2013
Available online 24 February 2013

Abstract

In recent years, monitoring offshore surface circulation in the Arctic Ocean with high frequency radars has become an issue of increasing practical importance. In this study, radar positions are optimized by minimizing the reconstruction errors of the surface currents in the Southeastern Chukchi Sea. By means of an adjoint sensitivity technique it is shown that in the case of a pair of radars, their optimal (i.e. most favorable) location is at Kivalina, a settlement near the strongest outflow of the Alaskan Coastal Current from the monitored domain. The least favorable location is at Shishmaref, a settlement near relatively weak inflow into the region as observed from the coast. However, if two pairs of radars are available, the best locations are Kivalina and Shishmaref. The results are verified using observational system simulation experiments (OSSEs) performed in the framework of a 4-dimensional variational assimilation of simulated radar observations into a numerical model. It is shown that correct specification of the first guess solution is of primary importance for obtaining realistic results from both adjoint sensitivity analysis and OSSEs. This emphasizes the necessity of obtaining accurate high resolution climatologies for future ice-free offshore regions in the Arctic.
Published by Elsevier B.V. and NIPR.

Keywords: Data assimilation; Optimization; Chukchi Sea; High frequency radar

1. Introduction

Rapid warming of the Arctic Ocean (Screen et al., 2012) is enabling an upward trend in commercial activity around its southern periphery where extended periods of ice-free conditions occur regularly. Increased human presence in the region inevitably results in a higher probability of accidents and environmental disasters, as well as contamination of the fragile Arctic environment by human waste. In order to prevent undesirable events and minimize their impact on the local ecology, there is a growing need to monitor the Southern Arctic by establishing observational networks along the coastal regions.

High frequency radar (HFR) is the key element of a modern observational network for coastal oceanography (e.g., Harlan et al., 2010). Located along the coast, these instruments provide surface wave and velocity data, which are among the most important

* Corresponding author. Tel.: +1 907 474 2680.
E-mail address: gleb@iarc.uaf.edu (G. Panteleev).

1873-9652/$ - see front matter Published by Elsevier B.V. and NIPR.
http://dx.doi.org/10.1016/j.polar.2013.01.001

sources of operational information about the ocean state. The advantage of the HFR is obvious: being deployed on the coast they do not need ship support and provide permanent data flow independent of the environmental conditions. Combined with satellite and *in situ* observations from gliders and stationary moorings, HFR data have been successfully used for hindcasting and monitoring of surface and subsurface circulation in the mid-latitude regions (e.g., Barth et al., 2010; Chavanne et al., 2007; Hisaki et al., 2001; Sentchev and Yaremchuk, 2007; Shay et al., 2008).

During the past five years, researchers have started to use HFRs in the Arctic. In particular, several HFRs have been deployed along the Northern Alaskan Coast and in the Eastern Chukchi Sea (Calder et al., 2009; Francis et al., 2010; Statscewich et al., 2009). Calder et al. (2009) pointed out that with an increase in marine transportation and offshore activities in the Arctic seas, HFRs will play a significant role in coastal velocity observations.

Since the Chukchi Sea, located in the Arctic Ocean region, is experiencing the most rapid decrease in ice cover (e.g., Kwok and Cunningham, 2010), it is becoming important to monitor its offshore regions. In particular, the Bering Strait may soon become the primary gateway for transportation between Europe and East Asia. From an academic point of view, accurate monitoring of the Bering Strait transport and circulation in the Chukchi and Beaufort Seas will benefit numerous scientific studies of climatological importance, such as Pacific–Arctic property exchange and long-term variations of freshwater storage in the Beaufort gyre. These and other criteria should be taken into account during planning of the Arctic Ocean HFR networks.

Currently there are several projects that use HFRs and gliders for the study of circulation in the Chukchi and Beaufort Seas (e.g., Francis et al., 2010; Potter et al., 2011; Winsor et al., 2011). These studies recommend the expansion of the HFR network in the South Eastern Chukchi Sea (SECS). In the present paper we attempt to optimize HFR locations with respect to the accuracy of reconstruction of the circulation in SECS, and explore the scenario in which four HFRs are deployed. Our study was initialized after deployment of one HFR in Red Dog Port during the summer of 2008, and discussion with local stakeholders. The study is focused on the reconstruction of surface currents because they are the key factor in forecasting the evolution of environmentally hazardous materials (floating debris, oil spills). Another reason is that surface flows strongly affect navigation conditions, which are important for ore transportation from Red Dog Port, and for transport between local settlements.

Taking into account that HFRs provide only surface velocity data, we explore two possibilities to specify the temperature and salinity fields. First, we mimic barotropic conditions by specifying homogeneous temperature and salinity distributions over the area. Second, the climatological temperature and salinity fields are utilized as background data. The study is based on the work of Panteleev et al. (2010) (hereinafter P10), who reconstructed climatological summer circulation in the Chukchi Sea using the 4-dimensional variational (4dVar) data assimilation approach.

Sensitivity of the data-optimized solutions to the HFR configurations was studied using the method of Köhl and Stammer (2004). Technically, this analysis is quite similar to the computation of the representative matrix elements that are extensively used in the data-space of 4dVar inversions (e.g., Bennett, 1992).

To check the validity of the results of the sensitivity analysis, a series of observational system simulation experiments (OSSEs) has been performed to analyze the quality of reconstructed SECS circulation using optimal HFR locations. Their results were compared with the results of similar experiments for non-optimal configurations. The impact of proper specification of temperature and salinity was also analyzed.

The remainder of this paper is organized as follows. We start with a description of the optimized SECS state obtained in P10 and present the theoretical background for the sensitivity analysis and the OSSE (Section 2). The results of adjoint sensitivity analysis of the surface circulation with respect to several prospective locations for HFR deployment are discussed in Section 3. In the same section, we validate these results using the OSSE technique. Finally, a discussion and conclusions are given in Section 4.

2. Methodology

2.1. Estimating the reference state

Configuration of the HFR sites is optimized by minimizing errors in reconstruction of the 1990 circulation observed in the SECS during the last navigable month of the year (October). The temporal evolution of the Chukchi Sea during September 1990–September 1991 was reconstructed by P10, who synthesized all available temperature, salinity, velocity and atmospheric observations in the framework of a regional primitive equation inverse model. The model

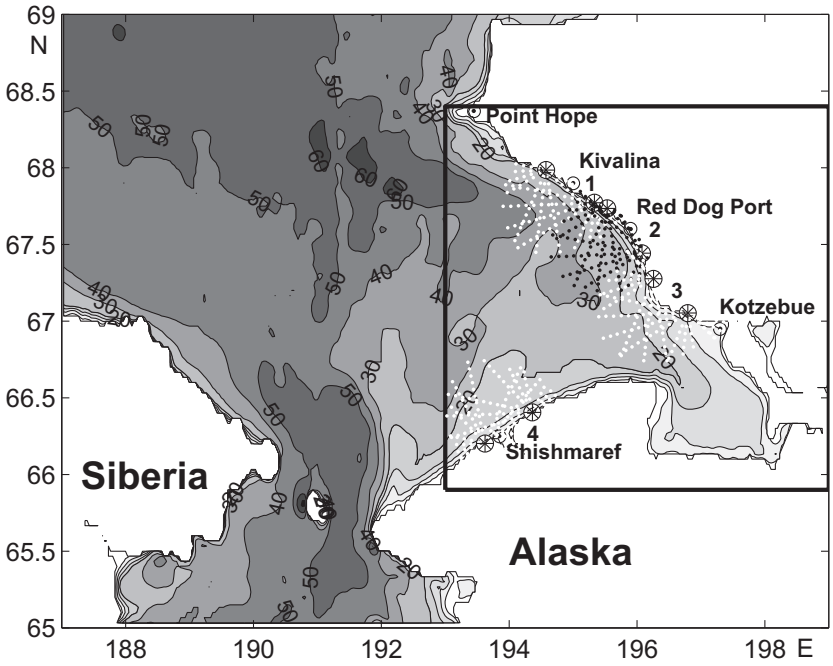

Fig. 1. Bottom topography of the Southern Chukchi Sea. The model domain is denoted by a bold rectangle. Circled asterisks denote pairs of the HFR sites considered in the study. Dotted lines schematically show regions covered by different pairs of radars.

is a modification of a C-grid z-coordinate Ocean General Circulation Model (OGCM) (Madec et al., 1999). It was successfully used for data-constrained 4dVar reconstructions of circulation in the Tsushima Strait (Nechaev et al., 2005), in the Barents Sea (Panteleev et al., 2006) and in the Kara Sea (Panteleev et al., 2007). The model was configured on a spherical grid with a mean resolution of 10 km in the horizontal, and 11 vertical levels with spacing varying between 2.5 m at the surface and 10 m near the bottom.

Technically, the data were interpolated in space and time by minimizing a cost function J that measured the distance between model fields and the data. The cost function includes quadratic model–data misfit terms and regularization terms penalizing squared Laplacians of the model fields. Minimization was done by varying a set of poorly known model parameters $\boldsymbol{c}$ (control variables) which included initial values of velocity, temperature and salinity, values of these fields at the open boundaries, and the corrections to the fluxes of

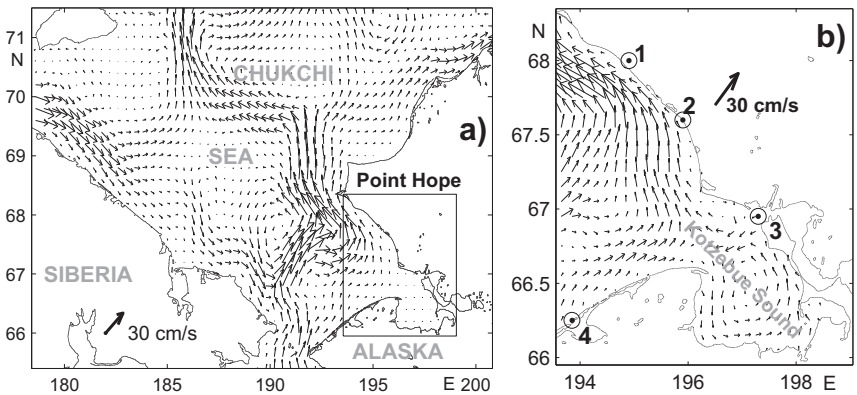

Fig. 2. Mean circulation in the Southern Chukchi Sea (a) and the Kotzebue Sound (b) averaged over 30 days spanning the integration time of the optimized solution in P10. Tested HFR site locations are shown by numbered circles (see Fig. 1) Numbers 1–4 designate Kivalina, Red Dog Port, Kotzebue and Shishmaref, respectively.

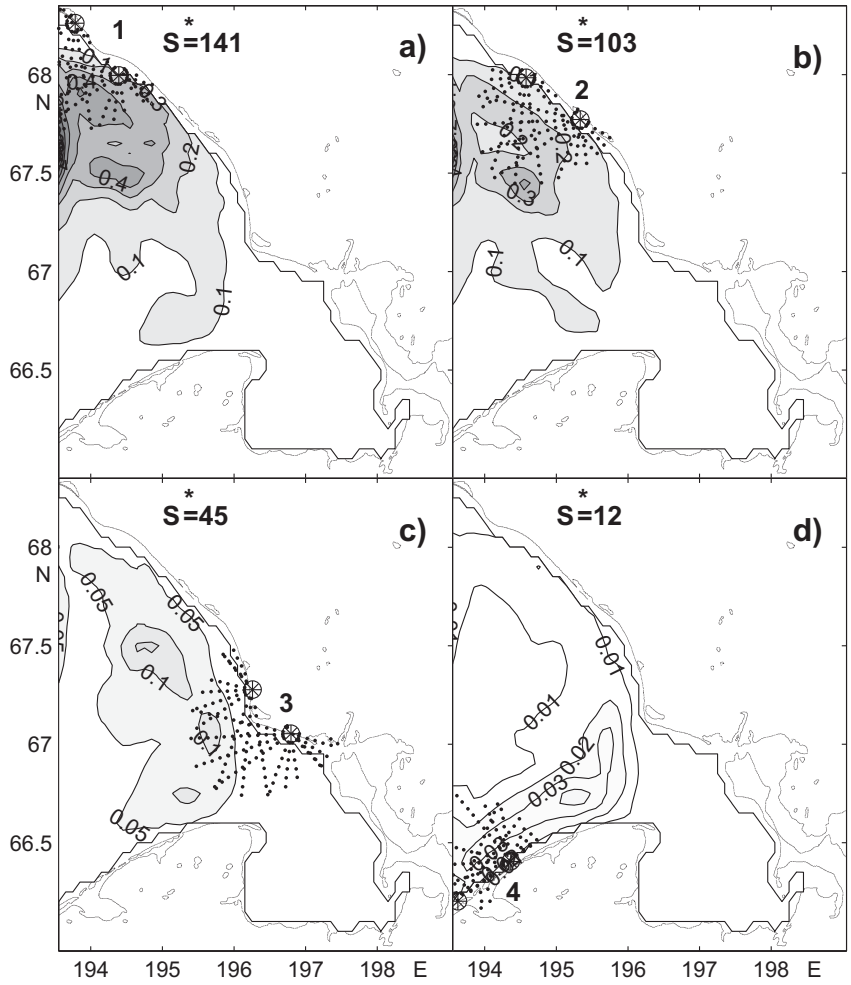

Fig. 3. Normalized sensitivities S computed as the magnitude of the response of the tangent linear model in the surface layer (0–10 m) to perturbations of the radial velocities observed by the HFRs in the four tested regions. The values of $S(x,y)$ were normalized by their maximum value shown in the upper left panel.

heat, salt and momentum at the ocean surface. The reconstructed Chukchi Sea circulation varies over a typical scale of 7–15 days under the optimized boundary forcing. Details of the reconstruction and analysis of the circulation can be found in P10.

In this study, the optimized solution of P10 was refined by increasing the model's horizontal resolution to 5 km. The model domain (Fig. 1) is embedded into the one used in P10, and the P10 solution interpolated into the 5 km grid was used as a first guess, while its coarse resolution (11 km) temperature, salinity and velocity fields were used as background observations. After that, the cost function was optimized in the same manner as in P10 over a time interval of 30 days (1–30 October, 1990).

Note that the local baroclinic Rossby radius is approximately 4–5 km. Thus, model resolution is insufficient to simulate eddies and other transient features, while variations of the large-scale circulation patterns are well reproduced. Such an intermediate resolution avoids instability of the linearized and adjoint models and makes the adjoint sensitivity analysis more robust (Section 2.2) (Bennett, 1992; Wunsch, 1996).

The optimized time-mean circulation in the Chukchi Sea (P10) and refined circulation in the SECS are shown in Fig. 2. Both are in qualitative agreement with previous modeling studies (e.g., Proshutinsky, 1986; Spaulding et al., 1987). The flow from the Bering Sea follows the northern coast of the Seaward Peninsula

towards Kotzebue Sound and outflows into the Chukchi Sea near Point Hope (Fig. 2a). In the model domain (Fig. 2b), the Bering Sea outflow is visible as two branches, entering the region at 66.3°N and 67.0–67.5°N. The southern branch contributes to the cyclonic gyre in the eastern Kotzebue Sound (66.5°N, 197°E) and then joins the northern branch near Red Dog Port (Fig. 2b).

2.2. Adjoint sensitivity analysis

The 4dVar data assimilation procedure transforms the *a priori* probability distribution for the data by injecting dynamical information and establishes correlations between any functionals of the ocean state variables described by the numerical model. In the framework of Gaussian statistics the *a posteriori* probability density in the vicinity of the optimal state is also Gaussian with the inverse covariance described by the Hessian matrix $\mathbf{H} = \partial^2 J/\partial \boldsymbol{c}^2$ of the assimilation problem. Therefore, the covariance between two quantities q_1, q_2, expressed in terms of the control variables $\boldsymbol{c}$ as $q_1 = \mathbf{L}_1\mathbf{X} \equiv \mathbf{L}_1\mathbf{M}\boldsymbol{c}$; $q_2 = \mathbf{L}_2\mathbf{X} \equiv \mathbf{L}_2\mathbf{M}\boldsymbol{c}$ is

$$\mathrm{cov}(q_1, q_2) = \mathbf{L}_2\mathbf{M}\mathbf{H}^{-1}\mathbf{M}^{\mathrm{T}}\mathbf{L}_1^{\mathrm{T}}, \tag{1}$$

where T denotes transposition, $\mathbf{M}$ is the model operator linearized in the vicinity of the optimal state, $\mathbf{L}_{1,2}$ are the linear functionals projecting ocean state $\mathbf{X} = \mathbf{M}\boldsymbol{c}$ on the observed quantities $q_{1,2}$ whereas the state vector $\mathbf{X} = \{u, v, T, S, \zeta\}$ lists the ocean field values (two components of the horizontal velocity vector, temperature, salinity and surface elevation) in all the grid points of the model space–time domain. The magnitude S of $|\mathrm{cov}\ (q_1,q_2)|^{1/2}$ can be used to estimate the sensitivity of a target quantity (say, q_1) to an observation of q_2 in the presence of other data and dynamical constraints, which define the structure of $\mathbf{H}$.

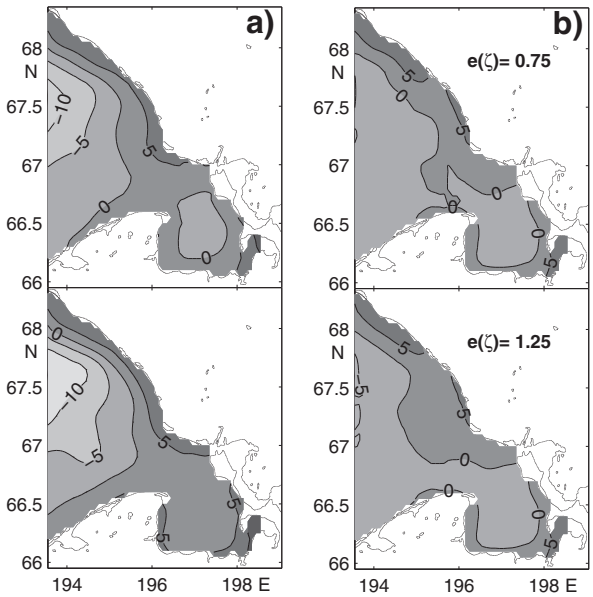

Fig. 4. The reference (a) and first guess (b) SSH fields (in cm) at day 6 (upper panels) and day 24 (lower panels) of the model integration. The mean SSH over the domain was removed. The value of $e(\zeta)$ is given in the center of the panels.

Following Köhl and Stammer (2004), we investigate the sensitivity of the optimized value of q_2 to observations of q_1 (i.e., the derivative $\partial q_1/\partial q_2$) under the assumption that the prior error variances $\boldsymbol{\sigma}_{\mathrm{c}}^2 \sim |\mathbf{H}^{-1}|$ of the control variables are much smaller than the combined observational and model error variances. This approximation does not explicitly take into account the new data used in the assimilation, which is quite reasonable for a new observational program where only prior statistics are available. The values of $\boldsymbol{\sigma}_{\mathrm{c}}$ were estimated as the root-mean-square (rms) variation of the reference solution. Under the simplifying assumption of Köhl and Stammer, the relationship for $S = |\mathrm{cov}\ (q_1,q_2)|^{1/2}$ reads

$$S = \left|\mathbf{W}^{-1}\mathbf{L}_2\mathbf{M}\mathbf{V}\mathbf{M}^{\mathrm{T}}\mathbf{L}_1^{\mathrm{T}}\right|^{1/2} \tag{2}$$

where $\mathbf{V}$ is the reference control error covariance (assumed to be diagonal $\mathbf{V} = \mathrm{diag}(\boldsymbol{\sigma}_{\mathrm{c}}^2)$) and $\mathbf{W}$ is the error variance in observing q_1.

In this study we assume that observation errors $\boldsymbol{\sigma}$ of q_1 are uncorrelated (i.e. $\mathbf{W} = \mathrm{diag}\ \boldsymbol{\sigma}(q_1)$) and known *a priori* while their values do not vary in space and time. Since we are interested in the normalized values of S, the actual value of $\boldsymbol{\sigma}(q_1)$ has no influence on the final results in this case. In Section 3.1, S is normalized by its maximum value over the entire set of the experiments.

We selected the target quantity q_2 as the monthly mean deviation of the SECS circulation from the reference evolution described in the previous section and computed its sensitivity to measuring radial velocities measured at the paired HFR sites; i.e., Eq. (2) was estimated consecutively for different combinations of operators $\mathbf{L}_1$ measuring the monthly mean radial velocities in the subdomains denoted by the dots shown in Fig. 1:

$$\mathbf{L}_1\mathbf{X} = \left\langle \sum (v_{\mathrm{i}}\boldsymbol{n}_{\mathrm{i}}) \right\rangle. \tag{3}$$

In Eq. (3), angular brackets denote the time average, and summation is over all surface velocity components v_{i} measured in the directions $\boldsymbol{n}_{\mathrm{i}}$ towards an HFR. Numerically, the components of $\mathbf{L}_2$ were used to force the adjoint model in its backward-in-time integration

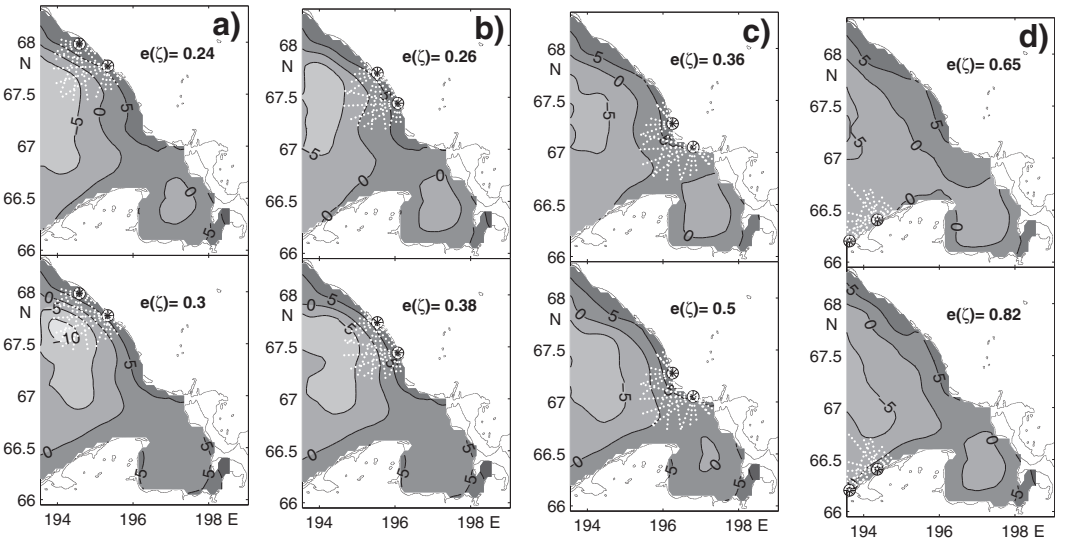

Fig. 5. SSH fields (cm) at day 6 (upper panels) and day 24 (lower panels) reconstructed by assimilating simulated velocity data from the HFRs positioned near Kivalina (a), Red Dog (b), Kotzebue (c) and Shishmaref (d) settlements. Climatological temperature and salinity were used as background fields. The values of $e(\zeta)$ for each panel are shown in the upper right.

over 30 days; the resulting values of the control perturbations were rescaled by **V** and used to force the tangent linear model during its forward-in-time integration for 30 days. Surface velocities of that run were compared with the "true" (reference) values, and their absolute difference was mapped to assess the impact of HFR observations. Note that the major impact on the mean circulation over the 30-day period was provided by the velocities at the open boundaries, which is consistent with a barotropic origin for the circulation in the major part of the Chukchi Sea (P10).

These computations made it possible to identify the SECS regions where radial velocities are likely to have the highest correlations with q_2 (reference surface velocities) in the framework of the model dynamics. From the observational point of view, these regions should have a higher priority for HFR deployment. Note that we tested only the logistically feasible HFR sites (Fig. 1), with HFR pairs located in the immediate proximity of the settlements (i.e., Kivalina, Red Dog Port, Kotzebue and Shishmaref).

2.3. Observational system simulation experiments

The OSSE technique is widely used for assessing the skill of data assimilation systems and the efficiency of the existing observational network in different regions (Lermusiaux et al., 2009; Vecchi and Harrison, 2007). The underlying idea is to simulate "data" using some reference model solution as a "true" ocean state, then to contaminate these data with noise (mimicking observational and model errors), and then reconstruct the "true state" from these data using the tested assimilation technique.

In the present study the radial surface velocity "data" mimicking the HFR observations were extracted from the non-stationary reference solution (Fig. 2b) described in Section 2.1. These data were then assimilated into the model. The assimilation procedure started from the first guess state, which was obtained by integrating model equations for 30 days starting from the state of rest and climatological temperature/salinity distributions. The model was forced by daily NCEP/NCAR atmospheric reanalysis products, and free radiation lateral boundary conditions were applied.

As a result of an OSSE, an optimal solution is obtained for an HFR configuration and then compared with the reference (true) solution. The metric used is the rms difference of the sea surface height (SSH) field. We are interested in retrieving (geostrophic) currents at time scales of several days or longer, and this metric is similar to the surface velocity metric, but is much more suitable for visualization. For this reason, we present the results in the following section in terms of the SSH distributions.

3. Results

3.1. Adjoint sensitivity analysis

Results of the sensitivity analysis are shown in Fig. 3. It is clear that where only two HFRs are

available, it is preferable to locate the HFRs in the region of Kivalina since the mean surface currents in the SECS are most strongly correlated with HFR observations in that region. The net impact of HFR observations was quantified by the integral parameter

$$S^* = \int S(x,y)\mathrm{d}x\mathrm{d}y, \tag{4}$$

whose value is shown at the top of the panels in Fig. 3. Here x and y denote horizontal coordinates and integration is performed over the entire model domain. Note that observations at Kivalina have the strongest impact on the reconstruction quality of the cyclonic SECS circulation pattern far upstream of the HFR site. This can be explained by the fact that the nearshore surface currents are partly forced by the north-westward coastal jet which originates in part from Kotzebue Sound, and a relatively weak inflow current near Shishmaref (Fig. 2b). Similar, but less pronounced effects are seen in the sensitivity maps for the Red Dog (Fig. 3b) and Kotzebue (Fig. 3c) configurations.

Placement of the HFRs at Shishmaref (Fig. 3d) appears to be the least effective in terms of capturing the SECS circulation ($S^* = 12$). This result can also be explained by the structure of the mean SECS circulation shown in Fig. 2: the main core of the along-shore north-westward current appears to be strongest and closest to the coastline in the Kivalina region, which is consistent with the local bottom topography (Fig. 1). As a result, observing the only outflow from (and most powerful flow within) the region provides information on the structure of the upstream currents. The relatively weak *inflow* currents in this relatively shallow region (Fig. 1) explain the low sensitivity to the HFR observations at Shishmaref.

The adjoint sensitivity maps in Fig. 3 are not additive and should not be used for analyzing the efficiency of the observing systems involving two or more pairs of HFRs. Although our goal was to optimize the location of one pair of HFRs, we conducted several experiments for the system based on two pairs of HFRs: the first at Kivalina, and the second at one of the three other settlements. It was found that HFR deployment at Kivalina and Shishmaref settlements is the most efficient. At first glance, the result appears to be somewhat counter-intuitive, since the Red Dog and Kotzebue sites demonstrate higher values of S^* (Fig. 3). However, an inspection of currents in Fig. 2b shows that observations at the Kivalina and Red Dog or Kotzebue sites are likely to be highly correlated with each other, as they measure essentially the same current that progresses along the coast. On the other hand, HFR observations at Shishmaref are weakly correlated with those at Kivalina, and therefore bring additional information into the assimilation algorithm.

Results of the sensitivity analysis are based on several rather restricting assumptions (linearization, Gaussianity of the probability density function, etc.), which may not be valid in reality. To assess the validity of our analysis we performed a series of OSSEs in the framework described in Section 2.3. The results of these experiments are given in the next section.

3.2. Observational system simulation experiments

Fig. 4 shows two snapshots of the SSH field corresponding to the reconstructed (reference) and the first guess solutions used in the OSSEs. The first guess solution (Fig. 4b) was obtained by integrating the model from the state of rest starting from the climatological-mean October distributions of temperature and salinity. These high resolution fields were derived from 20,369 temperature profiles collected in the Chukchi Sea between 1941 and 2008 (kindly provided by Dr. V. Luchin).

We conducted two series of OSSEs. In the first series, efficiencies of the two- and four-radar configurations were checked. In these experiments we utilized the above-mentioned climatological temperature and salinity fields to generate the first guess solution. The same fields were used as background observations in the cost function while assimilating HFR data. As described by P10, the baroclinic pressure gradient is usually 5–10 times smaller than the Coriolis term. Therefore, the use of climatological temperature and salinity fields as a background cannot produce a reference state without the correct specification of the barotropic and Ekman currents inferred by velocity observations from the HFR.

The reconstruction skill of the inverse model was tested by simulating radial velocity data corresponding to various HFR configurations. The following linear model for observed HFR radial velocities v was adopted:

$$v_\mathrm{i} = P^\mathrm{i}_\mathbf{n}\mathbf{v} + \mu V\varepsilon. \tag{5}$$

Here, $P^\mathrm{i}_\mathbf{n}$ denotes the linear interpolation operators, which project the gridded velocity vectors $\mathbf{v}$ onto the ith direction $\mathbf{n}$ at the HFR observation point $\boldsymbol{x}_\mathrm{i}$ from the apexes of the grid cell containing $\boldsymbol{x}_\mathrm{i}$. The term V is a typical magnitude of $\mathbf{v}$, ε is white noise with unit variance, and μ is the scalar parameter whose reciprocal is the signal-to-noise ratio. The value $\mu = 0.25$ was used within each series of OSSEs.

The error, $e(\zeta)$, between reconstructed and "true" SSH was estimated in a conventional manner:

$$e(\zeta) = \left[\int (\zeta - \zeta_{\text{true}})^2 \mathrm{d}x\mathrm{d}y \Big/ \int (\zeta_{\text{true}})^2 \mathrm{d}x\mathrm{d}y \right]^{1/2}, \qquad (6)$$

where $\boldsymbol{\zeta}(x,y)$ and $\boldsymbol{\zeta}_{\text{true}}(x,y)$ are the (demeaned) reconstructed and true SSH fields, respectively, and integration is performed over the entire model domain.

Fig. 5 shows the results of the OSSEs for the HFR pairs positioned near the four settlements shown in Fig. 1. The results appear to be in reasonable agreement with the adjoint sensitivity analysis (Fig. 3): the smallest errors, $e(\zeta)$, are observed when HFRs are placed in the Kivalina region, whereas deployment of the HFRs near Shishmaref demonstrates the least efficiency in terms of $e(\zeta)$. Interestingly, the SSH fields in Kotzebue Sound (Fig. 5a–d) are similar to the "true" SSH (Fig. 4a). In all of these maps, the SSH distribution corresponds to the weak cyclonic circulation defined by a 5 cm SSH drop between the coast and the central part of the Sound. This is probably caused by the regional baroclinic effects described by P10, and inferred from climatological temperature and salinity background fields in our experiments. Note also that the concept of adjoint sensitivity is based on the analysis of small disturbances propagated by the tangent linear model and its adjoint, while OSSEs are conducted using the fully non-linear ocean model. Therefore, a certain accumulation of the non-linear effects may be responsible for a larger SSH difference between the reference and the assimilation solutions in Kotzebue Sound at the end of the temporal assimilation window (compare discrepancies between the upper panels in Figs. 4a and 5 with those between the lower panels).

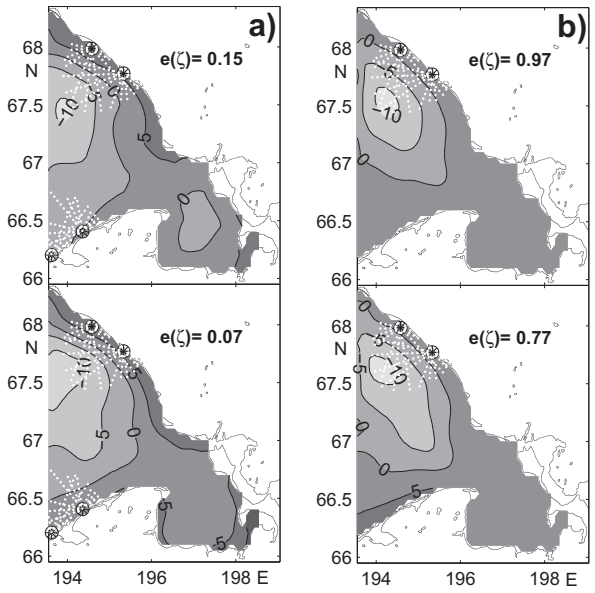

Fig. 6. (a) Same as in Fig. 5, but using velocity data from two pairs of HFRs located near Kivalina and Shishmaref. Climatological temperature and salinity were used as background fields. (b) Same as in Fig. 5a, but the reconstruction is performed with spatially uniform temperature and salinity background fields.

Results of an OSSE with four HFRs are shown in Fig. 6a. They indicate that the observing network based on four HFRs is several times more efficient than the system based on just one pair of HFRs near Kivalina. The resulting relative errors, $e(\zeta)$, do not exceed 15%, and are practically negligible (7%) near the end of the reconstructed period (day 24).

On the contrary, OSSEs with two HFR pairs both located at the northeastern coast of the domain (e.g., at Kivilina and Red Dog or Kotzebue) gave only an insignificant increase in the quality of the reconstructed currents with respect to the reconstruction based on one pair of HFRs in the Kivilina area: the corresponding error, $e(\zeta)$, decreased only by a factor of 1.2–1.3.

From the computational point of view, the OSSEs are more expensive than the adjoint sensitivity analysis because they involve a costly 4dVar assimilation process. However, these experiments provide quantitative estimates of the expected errors in reconstructing or monitoring the SECS circulation. Apart from the tested HFR configuration, these errors depend on the other factors that control the optimized solution. In particular, the values of $e(\zeta)$ may depend on the first guess and/or on the background fields used in the process of HFR data assimilation.

To assess the impact of the background, a series of OSSEs was conducted with the same HFR configuration, but with spatially uniform temperature and salinity distributions in the first guess solution and without the background temperature and salinity fields in the cost function. The open boundary conditions and atmospheric forcing were the same as in the "climatological" series of the OSSEs. Fig. 6b demonstrates a typical result from this series. The reconstruction errors are much larger, ranging between 70% and 100%. Thus, the accuracy of the background temperature and salinity fields appears to be important in obtaining reasonable estimates of the SECS circulation. The impact of the background temperature and salinity is twofold. First, the accurate distribution of temperature and salinity is important for accurate description of the baroclinic effects in certain parts (e.g., Kotzebue Sound) of the region (see for example, figure 16b in P10, also http://people.iarc.uaf.edu/~gleb/nsf_arctic_reanalysis1/2009JC005453.pdf). The importance of the baroclinic effects in summer and fall is a result of a) the influence of the Coastal Alaskan Current entering SECS along the Alaskan Coast

(Coachman et al., 1975), and of b) the accumulation of fresh and warm water in the Kotzebue Sound which joins the Coastal Alaskan Current and travels into the Chukchi Sea along the northeastern coast of the domain. Both of these effects play a dominant role in June–October, when atmospheric heating and river runoff reach their peak values. Second, the background temperature and salinity significantly constrain circulation by imposing a free-flow condition along the open boundary. Without this baroclinic constraint, and in the absence of adequate observations of the surface currents in the region(s) of HFR deployment, the optimal state has a tendency to form a rather unrealistic closed circulation (Fig. 6b).

4. Conclusions

Careful design of an observing system is crucial for effective monitoring of the ocean state, especially when the number of instruments is limited or they are expensive. In this study we have explored the possibility of monitoring ocean circulation in the SECS with an HFR observing network.

Using sensitivity analysis in the framework of a 4d variational data assimilation approach, the efficiency of HFR observations from four possible locations was analyzed. These locations are logistically defined by reasonable proximity to the major coastal settlements and ports in the SECS region. It was found that the optimal positioning of one HFR pair is near Kivalina, where the coastal current outflowing the domain reaches its maximum. The best configuration for two pairs involves HFR deployments in Kivalina and in Shishmaref, in the region of visible weak coastal inflow at the southwest of the domain. These HFR locations are promising because the villages can supply power to run the HFRs, and scheduled flights a couple of times per week provide easy accessibility.

Results of the sensitivity analysis were validated in the framework of OSSEs with noisy observations. As expected, optimal HFR positions revealed by the adjoint sensitivity analysis also demonstrated better observability of the SECS circulation.

Our results underline the importance of the background fields in the data assimilation procedures. It has been demonstrated that without a reasonable estimate of the background state, HFR observations are inefficient in monitoring the SECS circulation and provide accurate velocities only within the radar range. OSSEs demonstrated that the 4dVar data assimilation system with background climatologies is a powerful tool for projecting HFR observations offshore into the open sea regions. In this respect, we would like to emphasize the importance of developing high resolution climatologies for the regions where HFRs are planned for deployment in the near future.

In the examples described in this paper, optimal HFR locations are usually related to the coastal regions of the strongest regional inflows and outflows. However, this cannot be considered as a universal rule. As an example, experiments with HFR positioning between Kivalina and Point Hope have shown somewhat poorer efficiency of this configuration compared to observations from Kivalina despite the fact that coastal outflow northwest of Kivalina is even stronger. The explanation for this is that the observational efficiency is defined by the net correlation between the observations and the entire regional circulation. Usually, the stronger current correlates better with other circulation features, but formally this is not a rule. Therefore, analysis of the mean circulation pattern can be useful for suggesting the best configuration of the HFR network, but the final decision is best made after quantitative analysis using both the adjoint sensitivity and OSSE approaches.

Our model does not account for several mechanisms that may play an important role in regional dynamics (tides and tidally induced friction, river discharge, etc.). We believe, however, that optimal tuning of the model parameters largely compensates for this shortcoming achieved during the process of assimilating a large number of data; the background solutions shown in Figs. 2 and 4a represent rather realistic October scenarios. Consequently, the HFR locations in Figs. 3a and 6a are pretty likely to be optimal for long-term deployment.

We reported the results of adjoint sensitivity analysis and OSSEs for only a few positions of the HFR network based on radars with a range of 60 km. These positions were chosen due to the simplified logistics of their deployment. A similar study for other possible configurations and/or HFRs with larger ranges can be easily accomplished upon request. Similar numerical experiments could be conducted to assist in the planning of expeditions and observational networks in the Chukchi Sea and along the Arctic shelf break, where efficient monitoring of the flow is essential for progress in research in Arctic climate change, and for efficient monitoring of the coastal areas for practical purposes.

Acknowledgements

This study was supported by the Japan Agency for Marine-Earth Science and Technology (JAMSTEC) through their sponsorship of research activities at the International Arctic Research Center, and by the Office of Naval Research (Program element 0602435N,

project “Observational Impact”). G.P. was supported by the National Science Foundation (1107925 and 1203740) and by the North Pacific Research Board (NPRB) 828 award. M.Y. was supported by a grant from the BP/GOM Research Initiative through the Consortium for Advanced Research on Transport of Hydrocarbon in the Environment (CARTHE).

References

Barth, A., Alvera-Azcárate, A., Gurgel, K.-W., Staneva, J., Port, A., Beckers, J.-M., Stanev, E., 2010. Ensemble perturbation smoother for optimizing tidal boundary conditions by assimilation of high-frequency radar surface currents – application to the German Bight. Ocean Sci. 6, 161–178.

Bennett, A.F., 1992. Inverse Methods in Physical Oceanography. Cambridge University Press, Cambridge, 368 pp.

Calder, J., Proshutinsky, A., Carmack, E., Ashik, I., Loeng, H., Key, J., McCammon, M., Melling, H., Perovich, D., Eicken, H., Johnson, M.J., Rigor, I., 2009. Community White Paper: An Integrated International Approach to Arctic Ocean Observations for Society (a Legacy of the International Polar Year). http://www.oceanobs09.net/proceedings/cwp/cwp14/index.php.

Chavanne, C., Janekovic, I., Flament, P., Poulain, P.-M., Kuzmic, M., Gurgel, K.-W., 2007. Tidal currents in the northwestern Adriatic: high-frequency radio observations and numerical model predictions. J. Geophys. Res. 112, C03S21. http://dx.doi.org/10.1029/2006JC003523.

Coachman, L.K., Aagaard, K., Trip, R.B., 1975. Bering Strait: The Regional Physical Oceanography. Univ. of Washington Press, Seattle, 172 pp.

Francis, O., Atkinson, D., Weingartner, T., Panteleev, G., 2010. Accurate current and circulation monitoring through use of coastal radar stations and moorings in Alaska. In: Book of Abstracts Alaska Marine Science Symposium, Anchorage, AK, 18–22 January, p. 97.

Harlan, J., Terrill, E., Hazard, L., Keen, C., Barrick, D., Whelan, C., Howden, S., Kohut, J., 2010. The Integrated Ocean Observing System high-frequency radar network: status and local, regional, and national applications. Mar. Technnol. Soc. J. 44 (6), 122–132.

Hisaki, Y., Tokeshi, T., Fujie, W., Sato, K., Fujii, S., 2001. Surface current variability east of Okinawa Island obtained from remotely sensed and in situ observational data. J. Geophys. Res. 106 (C12), 31,057–31,073. http://dx.doi.org/10.1029/2000JC000784.

Köhl, A., Stammer, D., 2004. Optimal observations for variational data assimilation. J. Phys. Oceanogr. 34, 529–541.

Kwok, R., Cunningham, G.F., 2010. Contribution of melt in the Beaufort Sea to the decline in Arctic multiyear sea ice coverage: 1993–2009. Geophys. Res. Lett. 37, L20501. http://dx.doi.org/10.1029/2010gl044678.

Lermusiaux, P.F.J., Haley, P.J., Leslie, W.G., Logutov, O., Xu, J., Schmidt, H., Balasuriya, A., Benjamin, M., Petillo, S., Leslie, W.G., Gangopadhyay, A., Schmidt, A., 2009. OOI-OSSE09-MIT Home Page, http://mseas.mit.edu/Sea_exercises/OOI-OSSE09/index.html#forecasts.

Madec, G., Delecluse, P., Imbard, M., Lévy, C., 1999. OPA8.1 Ocean General Circulation Model. Reference Manual, Notes du Pôle de Modélisation. Institut Pierre Simon Laplace (IPSL), France, 91 pp.

Nechaev, D., Panteleev, G.G., Yaremchuk, M., 2005. Reconstruction of the circulation in the limited region with open boundaries: circulation in the Tsushima Strait. Oceanology 45 (6), 761–780.

Panteleev, G.G., Nechaev, D.A., Ikeda, M., 2006. Reconstruction of summer Barents Sea circulation from climatological data. Atmos. Ocean 44 (2), 111–132.

Panteleev, G., Proshutinsky, A., Kulakov, M., Nechaev, D.A., Maslowski, W., 2007. Investigation of the summer Kara Sea circulation employing a variational data assimilation technique. J. Geophys. Res. 112, C04S15. http://dx.doi.org/10.1029/2006JC003728.

Panteleev, G., Nechaev, D., Proshutinsky, A., Woodgate, R., Zhang, J., 2010. Reconstruction and analysis of the Chukchi Sea circulation in 1990–1991. J. Geophys. Res. 115, C08023. http://dx.doi.org/10.1029/2009JC005453.

Potter, R., Weingartner, T., Statscewich, H., Winsor, P., 2011. Surface current measurements in the northeast Chukchi Sea using shore-based HFR. In: Proc. Alaska Marine Symposium, Anchorage, AK, 17–21 January.

Proshutinsky, A., 1986. Calculation surge fluctuations in the level and circulation of water of the Chukchi Sea. Meteorol. Gidrologia 1, 54–61 (in Russian).

Screen, J.A., Deser, C., Simmonds, I., 2012. Local and remote controls on observed Arctic warming. Geophys. Res. Lett. 39, L10709. http://dx.doi.org/10.1029/2012GL051598.

Sentchev, A., Yaremchuk, M., 2007. VHF radar observations of surface currents off the northern Opal coast in the eastern English Channel. Cont. Shelf Res. 27, 2449–2464.

Shay, L.K., Seim, H.E., Savidge, D., Styles, R., Weisberg, R.H., 2008. High frequency radar observing systems in SEACOOS: 2002–2007 lessons learned. Mar. Technnol. Soc. J. 42 (3), 55–67. http://dx.doi.org/10.4031/002533208786842435.

Spaulding, M., Isaji, T., Mendelsohn, D., Turner, A.C., 1987. Numerical simulation of wind-driven flow through the Bering Strait. J. Phys. Oceanogr. 17, 1799–1816.

Statscewich, H., Potter, R., Atkinson, D., Francis, O., 2009. Collection of ocean current and wave height data from a CODAR in the southeastern Chukchi Sea, Alaska. In: Lessons from Continuity and Change in the Fourth International Polar Year Symposium, Inland Northwest Research Alliance and University of Alaska Fairbanks, Fairbanks, AK, 4–7 March.

Vecchi, G.A., Harrison, M.J., 2007. An observing system simulation experiment for the Indian Ocean. J. Clim. 20, 3300–3319.

Winsor, P., Statscewich, H., Weingartner, T., Potter, R., 2011. AUV glider missions in the Northeast Chukchi Sea. In: Proc. Alaska Marine Symposium, Anchorage, AK, January 17–21.

Wunsch, C., 1996. The Ocean Circulation Inverse Problem. Cambridge University Press, Cambridge, 442 pp.